

Article

Modification of Microstructure and Texture in Highly Non-Flammable Mg-Al-Zn-Y-Ca Alloy Sheets by Controlled Thermomechanical Processes

Sangbong Yi ^{1,*}, José Victoria-Hernández ¹, Young Min Kim ² , Dietmar Letzig ¹ and Bong Sun You ²

¹ Institute of Materials Research, Helmholtz-Zentrum Geesthacht, Max-Planck-Str. 1, 21502 Geesthacht, Germany; jose.victoria-hernandez@hzg.de (J.V.-H.); dietmar.letzig@hzg.de (D.L.)

² Implementation Research Division, Korea Institute of Materials Science, 797, Changwon-daero, Seongsan-gu, Changwon 51508, Korea; ymkim@kims.re.kr (Y.M.K.); bsyou@kims.re.kr (B.S.Y.)

* Correspondence: sangbong.yi@hzg.de; Tel.: +49-(0)4152-871911

Received: 28 December 2018; Accepted: 28 January 2019; Published: 2 February 2019



Abstract: The influence of rolling temperature and pass reduction degree on microstructure and texture evolution was investigated using an AZXW3100 alloy, Mg-3Al-1Zn-0.5Ca-0.5Y, in wt.%. The change in the rolling schedule had a significant influence on the resulting texture and microstructure from the rolling and subsequent annealing. A relatively strong basal-type texture with a basal pole split into the rolling direction was formed by rolling at 450 °C with a decreasing scheme of the pass reduction degrees with a rolling step, while the tilted basal poles in the transverse direction were developed by using an increasing scheme of the pass reduction degrees. Rolling at 500 °C results in a further distinct texture type with a far more largely tilted basal pole into the rolling direction. The directional anisotropy of the mechanical properties in the annealed sheets was caused by the texture and microstructural features, which were in turn influenced by the rolling condition. The Erichsen index of the sheets varied in accordance to the texture sharpness, i.e., the weaker the texture the higher the formability. The sheet with a tetrarchy distribution of the basal poles into the transverse and rolling directions shows an excellent formability with an average Erichsen index of 8.1.

Keywords: magnesium alloys; texture; formability; rolling

1. Introduction

In the last decades magnesium (Mg) alloys have been widely investigated due to their positive characteristics for a lightweight structure, e.g., their low density, high machinability and excellent damping capacity. However, the poor formability of Mg sheets, especially at room temperature, is one of the main drawbacks that retards the industrial application of semi-finished products. Conventional wrought Mg alloys, e.g., those based on the Mg-Al-Zn system such as the AZ31 alloy, have a tendency to develop strong basal-type textures during the sheet rolling process. The basal-type texture, in which most grains have their c-axes in the sheet normal direction (ND), causes a limited sheet formability from the restricted activities of the $\langle a \rangle$ dislocations slip, especially for the strain accommodation along the ND. The pyramidal $\langle c+a \rangle$ slip with a Burgers vector of $\langle 11-23 \rangle$ can accommodate the strain along the ND of such strongly textured material. Nevertheless, the $\langle c+a \rangle$ slip can be activated only at high temperature due to the high critical resolved shear stress (CRSS) at room temperature. To improve the formability of the Mg sheets, it is essential to provide a way of weakening the texture. In case of a weakened basal-type texture or non-basal texture components, it is expected that $\langle a \rangle$ dislocations with a relatively low CRSS contribute to accommodating the deformation along the ND. It was reported that texture weakening can be achieved by alloying Mg with yttrium (Y) and rare earth (RE) elements

such as cerium (Ce) or neodymium (Nd) [1–5]. Indeed, increased ductility, formability and strength have been observed in the sheet that has a weaker texture [6]. Even though the alloying addition of RE elements is an effective method of weakening textures and improving sheet formability at low temperature, the Mg alloy sheets with a reduced alloying amount or without RE elements, which are strategically important raw materials, are very beneficial from ecological and economic viewpoints.

The addition of Ca into Mg alloys is known to improve high temperature mechanical properties and ignition-proof behavior. Especially, the simultaneous addition of Ca with Y results in an excellent ignition-proof behavior and improved corrosion resistance. The Mg alloys with significantly improved non-flammability have attracted much attention for research activities and industrial applications [7–10]. Recent studies have shown that Ca addition also alters the strong basal-type texture to a more randomly distributed orientation after thermomechanical treatments, such as extrusion [11] or rolling [12,13], and, consequently improves room temperature formability. The Mg alloys containing Ca can be further strengthened by an optimized aging hardening scheme [14,15]. It is to be mentioned that the Ca added alloys investigated for wrought processes mostly handle with Al-free Mg alloys, e.g., Mg-Zn-Ca and Mg-Mn-Ca systems. Regarding further properties such as corrosion resistance and non-flammability, it is important to provide a method of texture weakening with a fine and homogeneous grain structure simultaneously in various alloy systems, especially in Mg alloys with Al addition. Moreover, studies on microstructure evolution during sheet processing and the mechanical behavior of the newly developed non-flammable alloy containing Ca and Y is limited.

In the present study, the microstructure and formability of the non-flammable AZXW3100 sheets, which are a modified AZ31 alloy by Ca and Y addition produced by different hot rolling schedules, were examined. A focus of the present study is to analyze the relationship between the thermomechanical process, microstructure evolution, and resulting properties.

2. Materials and Methods

The ingots of AZXW3100 alloy, with a nominal composition of Mg-3Al-1Zn-0.5Ca-0.5Y in wt.%, were cast into a steel mold under an Ar and SF6 atmosphere. The corresponding alloy compositions are well recognized for their excellent ignition resistance and high strength after extrusion [7,9], while their microstructure evolution during rolling and the resulting sheet properties have not been systematically studied. The cast ingot slabs with a thickness of 10 mm were machined and homogenized at 450 °C for 20 h under a continuous Ar flow. The homogenized slabs were rolled to a final gauge of 1 mm using different rolling conditions that are shown in Table 1. Two different schemes of deformation degree per pass were applied at the rolling temperatures of 450 °C and 500 °C; the deformation degrees per pass increased with the rolling step ($\varphi = 0.1$ to 0.3) or decreased with the rolling step ($\varphi = 0.3$ to 0.1).

Table 1. Different rolling conditions used in the present study.

Rolling Condition	Rolling Temperature (°C)	Deformation Degree per Pass (φ) (Total 11 Rolling Steps)	Remarks
450-inc	450	0.1 → 0.3 (increasing with rolling step)	$\varphi = -\ln(t_{(n+1)} / t_n)$ where, t_n = sheet thickness at the nth rolling step.
450-dec	450	0.3 → 0.1 (decreasing with rolling step)	
500-inc	500	0.1 → 0.3 (increasing with rolling step)	
500-dec	500	0.3 → 0.1 (decreasing with rolling step)	

The rolled sheets were annealed at 400 °C for different lengths of time, from 300 to 3600 s. The microstructure evolution during the rolling and recrystallization annealing were investigated with focus given to the influence of the different rolling schemes. Optical microstructures of the rolled and annealed sheets were observed by using standard metallographic sample preparation techniques and

an etchant based on picric acid [16]. Global texture measurements on the rolled and recrystallized sheets were conducted using X-ray diffraction (Cu K α , 40 kV and 40 mA, Panalytical, Almelo, The Netherlands). The orientation distribution function and complete pole figures were calculated by using a MATLAB toolbox MTEX [17] from six measured pole figures. Specimens for electron backscatter diffraction (EBSD) analysis were prepared by electropolishing in a Struers AC2 solution at $-20\text{ }^{\circ}\text{C}$ and 30 V. The EBSD measurements were conducted on a field emission gun scanning electron microscope (working at 15 kV, Zeiss Ultra 55, Carl Zeiss AG, Oberkochen, Germany) equipped with a Hikari detector (AMETEK Inc., Mahwah, NJ, USA) and an EDAX/TSL EBSD system.

The tensile samples were prepared from the sheets after recrystallization annealing in 3 different sheet directions: rolling direction (RD), transverse direction (TD) and 45° to RD, according to the DIN 50125 H12.5 \times 50. The quasi-static tensile tests were conducted at room temperature with an initial strain rate of 10^{-3} /s. The stretch formability of the sheets was examined by Erichsen tests of the as-rolled and annealed sheets at room temperature. The tests were performed using a punch with a diameter of 20 mm at a punch speed of 5 mm/min and a blank hold force of 10 kN, according to DIN 50101. The Erichsen index (IE) was determined by the punch stroke corresponding to the max load. The results from the tensile tests and the Erichsen tests are given as the average values from 3 samples, at least, for each condition of the examined sheet.

3. Results and Discussion

The optical microstructures, which are taken from longitudinal sections, and the recalculated (0001) and {10-10} pole figures of the AZXW3100 alloy sheets rolled with different conditions are shown in Figure 1, Figure 2, and Figure 5. The microstructural evolution during the recrystallization annealing at $400\text{ }^{\circ}\text{C}$ of each sheet is presented. The numbers given on the micrographs indicate the average grain sizes measured by the linear intercept method.

The sheet rolled with the 450-inc rolling scheme exhibits a strongly deformed structure with a large number of twin and deformation bands, which are homogeneously distributed in the whole sheet (Figure 1a). The grains are elongated in the RD. The average grain size of the rolled sheet is about $11\text{ }\mu\text{m}$, which is determined from the matrix grains without counting the twin boundaries. The annealed sheet at $400\text{ }^{\circ}\text{C}$ for 300 s shows a fully recrystallized microstructure with equi-axed grains and an average size of $6\text{ }\mu\text{m}$. The recrystallized grain structure is very stable and no significant grain growth occurs during the subsequent annealing, such that the grain size of the annealed sheet for 3600 s at $400\text{ }^{\circ}\text{C}$ is $8\text{ }\mu\text{m}$. Many of the fragmented secondary phases are aligned along the RD. They are observed in the as-rolled as well as the recrystallized sheets.

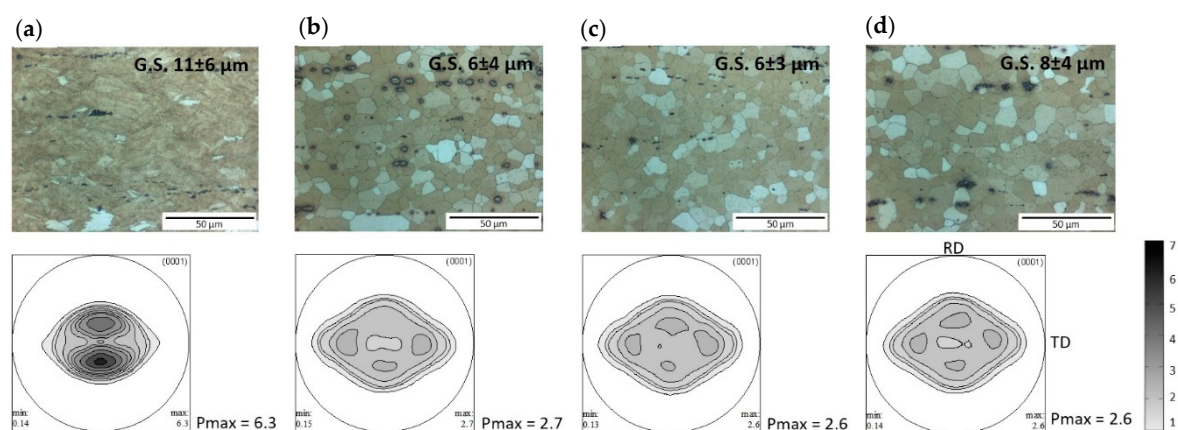


Figure 1. The optical micrographs and the recalculated (0002) pole figures of the sheets rolled by the 450-inc rolling scheme, i.e., the increasing deformation degrees with rolling step, (a) at the as-rolled condition and after annealing for (b) 300 s, (c) 600 s and (d) 3600 s at $400\text{ }^{\circ}\text{C}$.

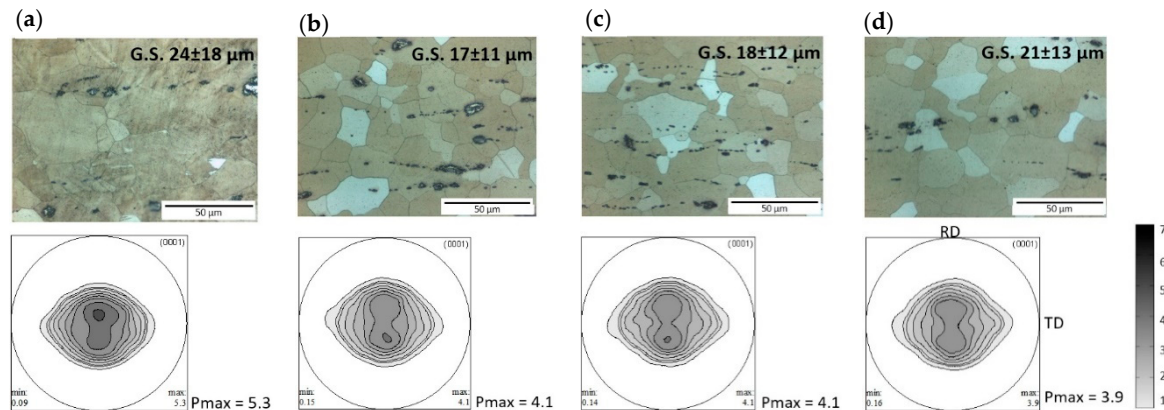


Figure 2. The optical micrographs and the recalculated (0002) pole figures of the sheets rolled by the 450-dec rolling scheme, i.e., the decreasing deformation degrees with rolling step, (a) at the as-rolled condition and after annealing for (b) 300 s, (c) 600 s and (d) 3600 s at 400 °C.

A relatively strong texture with a max pole density of the (0001) pole figure, $P_{\max} = 6.3$ multiple random distribution (m.r.d.), is obtained in the sheet rolled with the 450-inc scheme. The as-rolled sheet shows the basal pole distribution splitting into the RD. The formation of the texture component is understood as a result from a high activity $\langle c+a \rangle$ slip and secondary twinning during deformation [18]. The recrystallization annealing leads to a texture weakening such that the max pole density of the annealed sheet is $P_{\max} = 2.6$ m.r.d. Texture weakening accompanies the development of the basal pole split into the TD, while the basal poles in the RD become significantly weaker. This tendency of texture development, i.e., recrystallization texture with an additional basal pole split into the TD, has been mostly reported in studies of various RE or Ca containing Mg alloys sheets. It is important to note that the formation of weak textures with a TD basal pole split has been reported mostly in Al-free Mg alloys, such as Mg-Zn-RE and Mg-Zn-Ca systems. The present results show that such texture components are also obtained in Al-containing alloys by controlling the thermomechanical treatment conditions. This type of sheet texture stands out among others for its more homogeneous orientation distribution, which is usually more desirable for sheet metal forming processes than a texture with a predominant distribution of basal poles along one sheet direction.

Changing the rolling scheme produced a significantly different microstructure and texture in the final sheet. When decreasing the deformation degree with a rolling step, i.e., 450-dec rolling scheme with rolling degrees of $\varphi = 0.3$ at the beginning and $\varphi = 0.1$ at the final rolling steps, the rolled sheet showed a coarse grain structure with an average grain size of 24 μm . A fully recrystallized microstructure was shown after 300 s annealing at 400 °C, and the average grain size slightly varied from 18 μm to 21 μm during the recrystallization annealing up to 3600 s. The grain structure is relatively inhomogeneous, as shown by the relatively large values of the grain size deviation.

The as-rolled sheet shows the texture with a spread of the basal poles, up to about 20° tilting into the RD. That is, most grains have their basal planes aligning parallel to the sheet normal plane. The recrystallization annealing accompanied a slight weakening of the basal-type texture, from $P_{\max} = 5.1$ m.r.d. to $P_{\max} = 4.1$ m.r.d. at the as-rolled and recrystallized conditions, respectively. During the recrystallization annealing up to 3600 s at 400 °C the texture with the basal pole spread into the RD was maintained without a qualitative change. The sheet rolled by the 450-dec scheme shows a relatively stronger recrystallization texture, $P_{\max} = 3.9$ m.r.d. after 3600 s annealing, than the sheet rolled with the 450-inc scheme. Due to the low deformation degree at the final rolling steps the coarse grains formed during the intermediated annealing were kept without fragmentation by deformation, e.g., twinning and deformation bands. The grain structure and texture development during the post annealing of the 450-dec sheet seems to be related to the extended recovery-controlled process, such that no significant texture change resulted from the annealing. In contrast, the sheet rolled with a large deformation degree at the final rolling steps, e.g., the sheet rolled with the 450-inc

scheme, has a high deformation energy at the as-rolled condition. Thus, the recrystallization, including the nucleation, which is triggered mostly at highly deformed areas, like deformation bands, shear bands and grain boundaries, occurs during the annealing simultaneously with the extended recovery. This recrystallization process results in qualitative texture changes that accompany the weakening of deformation texture components.

The EBSD measurements clearly indicate the differences in the microstructure and deformation energy of the as-rolled sheets (Figure 3). The inverse pole figure (IPF) map and the kernel average misorientation (KAM) map of the EBSD measurement show the grain orientations and degree of deformation at measuring points. The KAM map is well acknowledged to represent the stored energy and geometrically necessary dislocations (GND) remaining in a deformed material. The rolled sheet by the 450-inc scheme, Figure 3a, shows a large number of twins, which correspond to the $\{10-12\}-\{10-11\}$ secondary twins determined by its orientation relationship to the matrix [19]. Moreover, the KAM map demonstrates that a relatively high deformation energy is distributed within the whole volume at the grain interior and along the grain boundaries, where a relatively higher deformed zone is observed along the lines inclined about 30° from the RD. The band-shaped structure is observed in the as-rolled sheet, marked with grey lines in Figure 3a. The band structure, at which the deformation energy is more concentrated, mostly develops along the twins and seems to be a microstructural feature prior to the shear band. The sheet rolled by the 450-dec scheme shows a deformed microstructure with twins. However, the degree of deformation is much lower than that of the 450-inc sheet. The KAM map also indicates that the deformation degree is more or less concentrated along the grain and twin boundaries. The elements distribution maps at the same area to the EBSD measurement of the 450-dec sheet are shown in Figure 4. It is obvious that the secondary phases observed in the examined alloy, which are shown as black dots in the EBSD maps, are mostly the high Al-Ca and Al-Y phases, e.g., $(Al, Mg)_2Ca$ and Al_4Mg_4Y . A relatively high concentration of Mn, 2~5 wt.% from the EDX analysis, was found at the Al_4Mg_4Y phase.

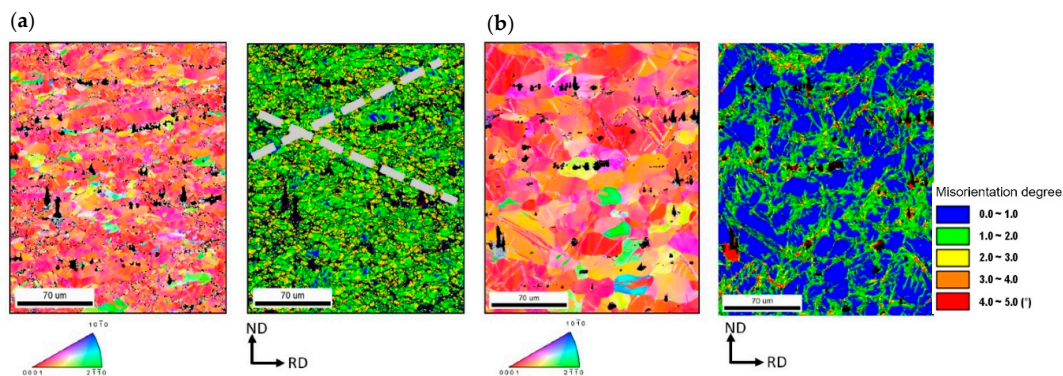


Figure 3. EBSD inverse pole figure maps and kernel average misorientation maps of the as-rolled sheets by (a) 450-inc and (b) 450-dec rolling schemes.

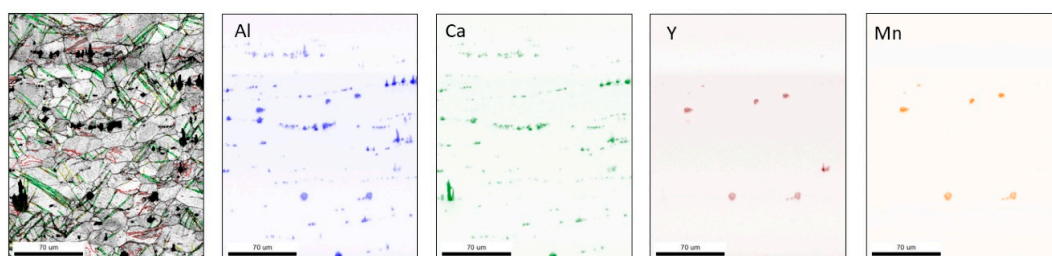


Figure 4. Grain boundary map and alloying elements distribution maps of the as-rolled sheet by 450-dec rolling scheme, at the same measuring area with the Figure 3b. Different colors of the boundaries, in the grain boundary map, correspond to the twin types: red to $\{10-12\}$ extension, yellow to $\{10-11\}$ contraction and green to $\{10-12\}-\{10-11\}$ secondary twins.

The influence of the rolling scheme with regards to the step reduction degree on the microstructure and texture evolution is negligible, when the sheet rolling is conducted at a higher temperature. The sheets rolled at 500 °C have a distinct texture type, where the basal pole split into the RD with a tilting angle of 20~30° from the ND is formed independently from the step reduction degree (Figure 5a,c). After annealing for 600 s at 400 °C, the texture weakens to $P_{\max} = 3.6$ and 3.4 in the 500-inc and 500-dec sheets, respectively. This type of texture with the basal pole split into the RD and a relatively weaker intensity compared to a commercial Mg alloy is generally observed in the Mg-REE binary alloy sheets [20]. The grain sizes of the annealed sheets, 9 μm and 7 μm , are comparable to those of the 450-inc sheet. Besides the intermetallic particles, many stringer structures of oxide inclusions, identified by means of EDX analysis, are found along the RD in the optical micrographs, and also in the sheets rolled at 450 °C. These microstructural features originate from the casting defects, e.g., micro-voids and oxide inclusions, which are elongated during the rolling procedures.

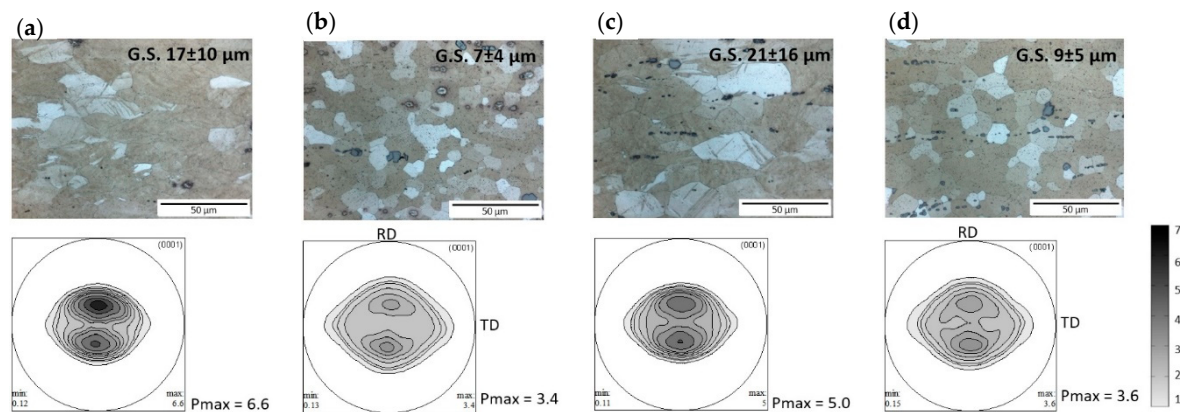


Figure 5. The optical micrographs and the recalculated (0002) pole figures of the sheets rolled by the 500-inc and 500-dec schemes, (a), (c) as-rolled condition and (b), (d) after annealing for 600 s at 400 °C, respectively.

Figure 6 displays the stress strain curves during the uniaxial tensile tests of the annealed 450-inc and 450-dec sheets in three sheet planar directions, at RD, TD, and 45° from the RD. The mechanical properties of the sheets are listed in Table 2. The higher strength and ductility of the 450-inc sheet are associated with a finer grain structure and weaker texture than those of the 450-dec sheet. Due to this weak texture, i.e., the more randomly distributed orientations, the dislocation slip can be more easily activated without a geometrical restriction, i.e., a higher Schmid's factor for the basal $\langle a \rangle$ slip than a more strongly textured material, such that higher ductility is achieved based on a homogeneous deformation. The 450-inc sheet has a high yield strength ($\sigma_{0.2} > 150$ MPa) in different sheet planar directions. Moreover, other alloys sheets that have a similar texture, e.g., the ZE10 sheet in [21], have a much lower strength, especially in the TD. The anisotropic mechanical properties of the sheets can also be understood from the texture. The higher stress values in the RD than the TD are associated with the broader angular tilt of the basal poles towards the TD than the RD. Due to its geometrical advantages, the basal $\langle a \rangle$ slip is more favored during the tensile loading in the TD. The directional anisotropy in the yield strength is larger in the 450-inc sheet, which is attributed to the basal pole split into the TD. The 450-dec sheet shows a basal pole spread into the TD and, accordingly, the smaller directional anisotropy of the yield strength is observed. Indeed, it is expected that the anisotropy in ductility is insignificant, even with a slightly higher ductility in the TD [21]. In general, the sheet planar direction with lower stress corresponds to higher uniform strain and fracture strain. The premature fracture during the tension in the TD of the present study was caused by the oxide inclusions aligned along the RD. The stringers of the oxide inclusions act as a stress concentration site, especially during the loading along the TD, such that the fracture occurs at a low strain level, as also shown in a previous study [22].

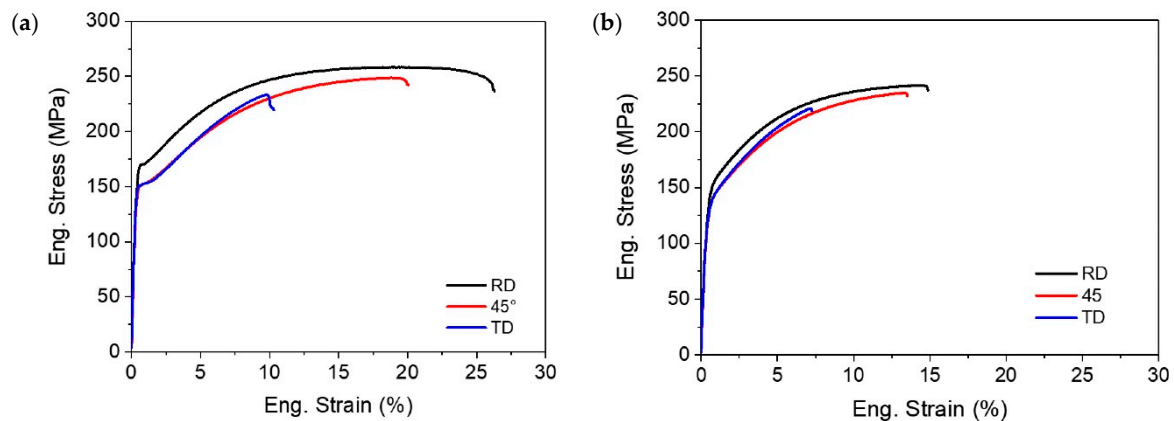


Figure 6. Stress strain curves of the annealed sheets for 600 s at 400 °C after rolling by (a) 450-inc and (b) 450-dec schemes.

Table 2. Mechanical properties of the annealed sheets from tensile tests.

Tensile Properties	Annealing for 600 s at 400 °C					
	450-inc			450-dec		
	RD	45°	TD	RD	45°	TD
Yield strength (MPa)	166 ± 6.7	151 ± 1.7	150 ± 0.9	149 ± 0.1	138 ± 0.9	137 ± 0.3
Tensile strength (MPa)	258 ± 1.0	243 ± 8.0	224 ± 12.2	242 ± 1.6	235 ± 0.9	204 ± 23.8
Fracture strain (%)	25.0 ± 1.8	17.0 ± 5.2	8.9 ± 2.0	14.4 ± 0.6	12.2 ± 0.6	4.7 ± 2.5
Uniform elongation (%)	18.0 ± 1.1	15.0 ± 4.7	8.1 ± 1.6	13.9 ± 0.6	12.0 ± 0.5	4.6 ± 2.4

Figure 7 presents the Erichsen index (IE) of the as rolled and annealed sheet samples. The as-rolled sheets show very low formability, $IE = 2.5 \sim 3$, independently on the rolling scheme. After annealing for 600 s at 400 °C, improved formability, which is related to the reduction of lattice defects and the texture weakening, is achieved. A remarkable improvement of the formability is obtained in the 450-inc sheet after annealing. The average IE of 8.1 is almost a three-fold higher value in comparison to the commercial AZ31 sheet ($IE = 2 \sim 3$). Other sheets, rolled at 500 °C and 450-dec, have an IE of 4.0~4.5 after annealing. The excellent stretch formability of the 450-inc sheet after recrystallization annealing is attributed to the weak texture and the basal pole split into the RD and TD. As mentioned above, this texture type with a tetrarchy distribution of the basal poles is advantageous for the material flow in the sheet thickness direction during stretch forming due to the high activity of the basal $\langle a \rangle$ slip. Additionally, the fine grain structure with an average grain size of 6 μm and fine particles distributed homogeneously also enhance sheet formability. Considering that a large number of stringers of the secondary phase particles and Mg oxide aligning along the RD are found in all samples, we consider that the ductility in the TD and the stretch formability could be further improved. This requires the further optimization of the alloy composition as well as the improved casting technology. For instance, casting under vacuum or a controllable solidification rate ensures the reduced interaction between the melt and atmosphere.

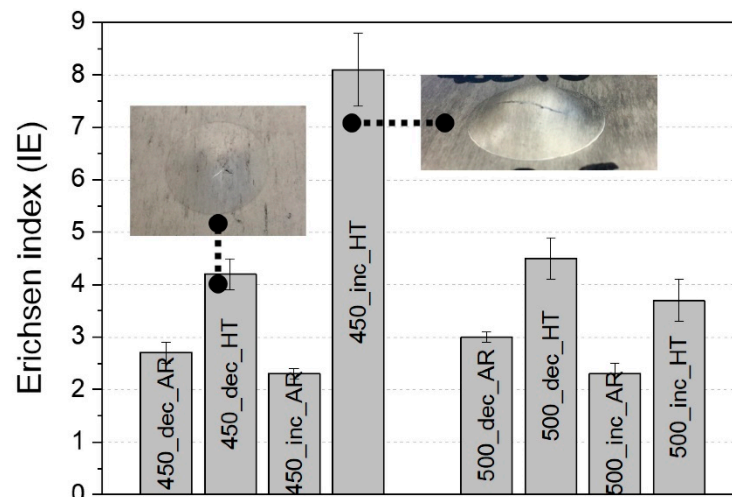


Figure 7. Erichsen index of the differently rolled and annealed sheets and appearances of the Erichsen samples of the 450-dec and 450-inc sheets (inset).

4. Summary

Non-flammable AZXW3100 alloy sheets were produced using various rolling conditions. Depending on the rolling schedule, distinct microstructure and texture evolution was observed during the warm rolling and subsequent recrystallization annealing.

The texture with tetrarchy characteristics, i.e., the basal pole split into TD and RD simultaneously, developed after rolling at 450 °C, with the deformation degree per pass increasing with the rolling step. The rolling at 450 °C with a decreasing deformation degree per pass resulted in a coarse grain structure with a relatively strong basal-type texture. After the sheet rolling at 500 °C, the texture with the basal pole split into the RD was developed, while the influence of the deformation degree per rolling step on the microstructure and texture became negligible.

The directional anisotropy of the mechanical properties is related to the distinct texture of each rolled sheet. It is obvious that the AZXW3100 sheet that has a weak texture with the basal pole split into the TD shows excellent sheet formability.

The present results clearly indicate that a highly ductile and formable sheet can be produced by microstructure and texture control, which in turn originate from optimized thermomechanical treatments. Further studies on deformation and recrystallization mechanisms in correlation with thermomechanical treatments will identify the fundamental mechanisms that produce such variety in microstructure and texture development.

Author Contributions: Experimental works were carried out by S.Y., J.V.-H. with continuous discussion with Y.M.K., B.S.Y. and D.L. All authors discussed the experimental results and the conclusions, and reviewed the present manuscript.

Acknowledgments: The authors appreciate A. Reichart and Y.K. Shin at HZG for technical support during the warm rolling and microstructure analysis. The financial support of the NST-National Research Council of Science & Technology (No. CRC-15-06-KIGAM) by the Korea government (MSIP) is gratefully acknowledged.

References

- Bohlen, J.; Nürnberg, M.R.; Senn, J.W.; Letzig, D.; Agnew, S.R. The texture and anisotropy of magnesium-zinc-rare earth alloy sheets. *Acta Mater.* **2007**, *55*, 2101–2112. [[CrossRef](#)]
- Stanford, N.; Barnett, M. Effect of composition on the texture and deformation behaviour of wrought Mg alloys. *Scr. Mater.* **2008**, *58*, 179–182. [[CrossRef](#)]
- Chino, Y.; Kado, M.; Mabuchi, M. Enhancement of Tensile Ductility and Stretch Formability of Magnesium by Addition of 0.2 wt%(0.035 at%)Ce. *Mater. Sci. Eng.* **2008**, *A494*, 343–349. [[CrossRef](#)]

4. Bohlen, J.; Cano, G.; Drozdenko, D.; Dobron, P.; Kainer, K.U.; Gall, S.; Müller, S.; Letzig, D. Processing Effects on the Formability of Magnesium Alloy Sheets. *Metals* **2018**, *8*, 147. [[CrossRef](#)]
5. Tekumalla, S.; Seetharaman, S.; Almajid, A.; Gupta, M. Mechanical Properties of Magnesium-Rare Earth Alloy Systems: A Review. *Metals* **2015**, *5*, 1–39. [[CrossRef](#)]
6. Yi, S.; Bohlen, J.; Heinemann, F.; Letzig, D. Mechanical anisotropy and deep drawing behaviour of AZ31 and ZE10 magnesium alloy sheets. *Acta Mater.* **2010**, *58*, 592–605. [[CrossRef](#)]
7. Kim, Y.M.; Kim, H.S.; You, B.S.; Yim, C.D. Non-Flammable Magnesium Alloy with Excellent Mechanical Properties, and Preparation Method Thereof. U.S. Patent 2013/0183193 A1, 18 July 2013.
8. Gneiger, S.; Papenberg, N.; Frank, S.; Gradinger, R. *Investigations on Microstructure and Mechanical Properties of Non-Flammable Mg–Al–Zn–Ca–Y Alloys, Magnesium Technology 2018, TMS Annual Meeting & Exhibition, Phoenix, USA, March 11–15, 2018*; Orlov, D., Joshi, V., Solanki, K.N., Neelameggham, N.R., Eds.; Springer: Berlin/Heidelberg, Germany, 2018. [[CrossRef](#)]
9. Go, Y.; Jo, S.M.; Park, S.H.; Kim, H.S.; You, B.S.; Kim, Y.M. Microstructure and mechanical properties of non-flammable Mg-8Al-0.3Zn-0.1Mn-0.3Ca-0.2Y alloy subjected to low-temperature, low-speed extrusion. *J. Alloys Compd.* **2018**, *739*, 69–76. [[CrossRef](#)]
10. You, B.S.; Kim, Y.M.; Yim, C.D.; Kim, H.S. *Oxidation and Corrosion Behavior of Non-Flammable Magnesium Alloys Containing Ca and Y. Magnesium Technology 2014, TMS Annual Meeting & Exhibition, San Diego, USA, Feb. 16–20, 2014*; Alderman, M., Manuel, M.V., Hort, N., Neelameggham, N.R., Eds.; Springer: Berlin/Heidelberg, Germany, 2014. [[CrossRef](#)]
11. Stanford, N. The effect of calcium on the texture, microstructure and mechanical properties of extruded Mg–Mn–Ca alloys. *Mater. Sci. Eng.* **2010**, *A528*, 314–322. [[CrossRef](#)]
12. Kim, D.W.; Suh, B.C.; Shim, M.S.; Bae, J.H.; Kim, D.H.; Kim, N.J. Texture Evolution in Mg-Zn-Ca Alloy Sheets. *Metall. Mater. Trans.* **2013**, *A44*, 2950–2961. [[CrossRef](#)]
13. Chino, Y.; Huang, X.; Suzuki, K.; Mabuchi, M. Enhancement of Stretch Formability at Room Temperature by Addition of Ca in Mg-Zn Alloy. *Mater. Trans.* **2010**, *51*, 818–821. [[CrossRef](#)]
14. Bhattacharjee, T.; Suh, B.C.; Sasaki, T.T.; Ohkubo, T.; Kim Nack, J.; Hono, K. High strength and formable Mg–6.2Zn–0.5Zr–0.2Ca alloy sheet processed by twin roll casting. *Mater. Sci. Eng.* **2014**, *A609*, 154–160. [[CrossRef](#)]
15. Hofstetter, J.; Becker, M.; Martinelli, E.; Weinberg, A.M.; Mingler, B.; Kilian, H.; Pogatscher, S.; Uggowitzer, P.J.; Löffler, J.F. High-Strength Low-Alloy (HSLA) Mg–Zn–Ca Alloys with Excellent Biodegradation Performance. *JOM* **2014**, *66*, 566–572. [[CrossRef](#)]
16. Kree, V.; Bohlen, J.; Letzig, D.; Kainer, K.U. The metallographical examination of magnesium alloys. *Pract. Metallogr.* **2004**, *41*, 233–246.
17. MTEX Toolbox. Available online: <http://mtextoolbox.github.io/> (accessed on 28 December 2018).
18. Agnew, S.R.; Yoo, M.H.; Tomé, C.N. Application of texture simulation to understanding mechanical behavior of Mg and solid solution alloys containing Li or Y. *Acta Mater.* **2001**, *49*, 4277–4289. [[CrossRef](#)]
19. Al-Samman, T.; Gottstein, G. Room temperature formability of a magnesium AZ31 alloy: Examining the role of texture on the deformation mechanisms. *Mater. Sci. Eng.* **2008**, *A488*, 406–414. [[CrossRef](#)]
20. Hantzsche, K.; Bohlen, J.; Wendt, J.; Kainer, K.U.; Yi, S.B.; Letzig, D. Effect of rare earth additions on microstructure and texture development of magnesium alloy sheets. *Scr. Mater.* **2010**, *63*, 725–730. [[CrossRef](#)]
21. Stutz, L.; Bohlen, J.; Kurz, G.; Letzig, D.; Kainer, K.U. Influence of the processing of magnesium alloys AZ31 and ZE10 on the sheet formability at elevated temperature. *Key Eng. Mater.* **2011**, *473*, 335–342. [[CrossRef](#)]
22. Suh, J.; Victoria-Hernández, J.; Letzig, D.; Golle, R. Effect of processing route on texture and cold formability of AZ31 alloy sheets processed by ECAP. *Mater. Sci. Eng.* **2016**, *A669*, 159–170. [[CrossRef](#)]

